SUPPLEMENTARY MATERIAL

Deciphering the Luminescence Spectral Shape of Oxyluciferin's Analogue Through a Mixed Quantum Classical Approach

Houda Moumene,[a] Giacomo Prampolini, [b] Cristina García-Iriepa, [c] Javier Cerezo, [d,*], Isabelle Navizet, [a,*] and Fabrizio Santoro [b,*]

[a] *Univ Gustave Eiffel, Univ Paris Est Creteil, CNRS*,
UMR 8208, MSME, F-77454 Marne-la-Vallée, France
[b] *Istituto di Chimica dei Composti OrganoMetallici* (ICCOM-CNR),
Area della Ricerca, via G. Moruzzi 1, I-56124 Pisa, Italy
[c] *Universidad de Alcalá,*
Departamento de Química Analítica, Química Física e Ingeniería Química,
Functional Molecular Systems (FuMSys) group,
Ctra. Madrid-Barcelona, Km. 33.600, 28805, Alcalá de Henares, Madrid, Spain
[d] *Departamento de Química* and *Institute for Advanced Research in Chemical Sciences (IAdChem)*,
Universidad Autónoma de Madrid, 28049 Madrid, Spain

[*]email: fabrizio.santoro@pi.iccom.cnr.it, isabelle.navizet@univ-eiffel.fr, javier.cerezo@uam.es

Contents

S1 Methods

S1.1 JOYCE Parameterization

The intra-molecular energy term E^{intra}_{QMD-FF} parameterization has been derived from the QM databases (equilibrium geometry, its Hessian matrix, relaxed torsional energy scan for S_0 and S_1 for each considered functional) by means of the JOYCE code.[1] As mentioned in the main text, according to the JOYCE approach,[2,3] the redundant internal coordinates (RICs) chosen to represent the target molecule dynamics are classified into two different sets: stiff ($\mathbf{r}^{ric}$) or flexible ($\mathbf{R}^{ric}$), depending whether rather small displacements from the equilibrium geometry or large amplitude motions are to be expected.

The intramolecular QMD-FF term is hence therefore further partitioned in several contributions, namely

$$E^{intra}_{QMD-FF} = E_s + E_b + E_{st} + E_{ft} \tag{S1}$$

The first three terms refer to $\mathbf{r}^{ric}$, and can be approximated through harmonic potentials, *i.e.*

$$E_s = \frac{1}{2}\sum_{s}^{N_s} k_s (r - r^0)^2 \; ; \; E_b = \frac{1}{2}\sum_{b}^{N_b} k_b (\theta - \theta^0)^2 \; ; \; E_{st} = \frac{1}{2}\sum_{st}^{N_{st}} k_{st} (\phi - \phi^0)^2 \tag{S2}$$

It is worth noticing that while the first two terms, *i.e.* the stretching and bending contributions E_s and E_b, are widely used by popular general purpose FFs, E_{st} is seldom employed for describing torsions of stiff dihedral angles. Yet, it appears to be better suited to account for the internal energy due to small and fast distortions of a dihedral ϕ from its equilibrium position ϕ^0, and the JOYCE procedure routinely employs such description, to mimic the behaviour of stiff and fast vibrating torsions, as those ruling the planarity of aromatic rings or conjugated double bonds[4–7] or the octahedral symmetry of a metal-organic complex.[8–10] The last term of equation (S1) is instead assigned to the flexible internal coordinates. In the present study E_{ft} only depends on the dihedral δ (see Figure S1.b), which is expected to experience larger distortion during simulation, and should be tackled beyond the harmonic approximation.

Concretely,

$$E_{ft} = \sum_{j}^{N_{cos}} k_j^{ft} \left[1 + cos(n_j \delta - \gamma_j)\right] \tag{S3}$$

where k_j^{st}, n_j and γ_j are the force constant, multiplicity and phase of each cosine term considered in the sum. It is worth noticing that, given the overall stiffness of the **cproxy**$^-$'s scaffold,

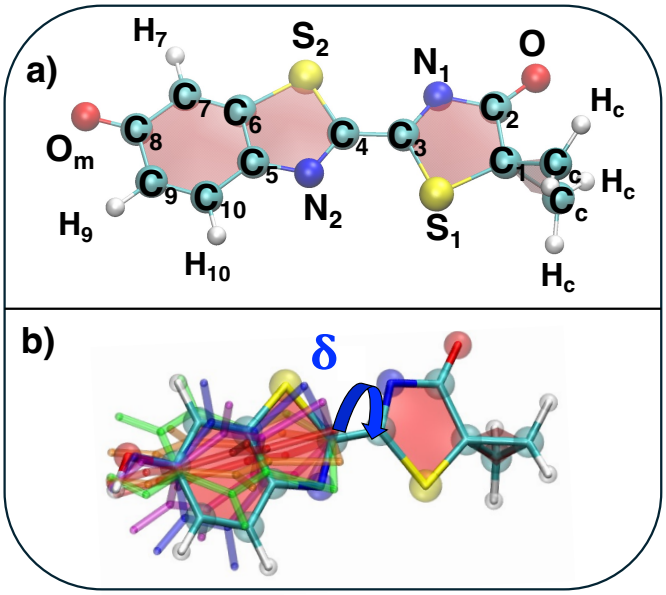

Figure S1: Atom types and flexible dihedral definition adopted for **cproxy**$^-$ during JOYCE parameterizations. a) atom labels; b) intra-ring flexible dihedral δ and the effect of its rotation.

specific intramolecular nonbonded interactions are not explicitly required, since the distance between far lying atoms are not expected to be altered significantly during dynamics. In this framework, the JOYCE parameterization strategy allows to switch off such interactions, and limits the use of both charge-charge and Lennard-Jones (LJ) terms to the sole solute-solvent and solvent-solvent interactions (see also main text).

The JOYCE parameterization is carried out by a least-square linear fitting,[2] thus minimizing the objective function

$$I^{intra} = \sum_{K \leq L}^{3N-6} \frac{2W''_{KL}}{C} \left[H_{KL} - \left(\frac{\partial^2 E^{intra}_{QMD-FF}}{\partial Q_K \partial Q_L} \right) \right]^2_{g_0} + \sum_{g}^{N_{geom}} W_g \left[\Delta U - E^{intra}_{QMD-FF} \right]^2_g \tag{S4}$$

In the first term on the right side of equation (S4), the sum runs over the 3N-6 dye's coordinates, C is a normalization factor, Q_K is the K^{th} QM normal mode, whereas H_{KL} and $\frac{\partial^2 E^{intra}_{QMD-FF}}{\partial Q_K \partial Q_L}$ are QM and QMD-FF Hessian matrix elements, both evaluated in the minimum energy geometry (g_0). The normalized diagonal elements of the weight matrix $\mathbf{W}''$ are fixed, as in previous applications, at twice the value of those corresponding to the off diagonal terms. In the second term, ΔU and E^{intra}_{QMD-FF} are respectively the QM computed energy difference between the g and g_0 geometries, and the QMD-FF energy computed at the g geometry through equation (S1); N_{geom} is the number of the different geometrical arrangements sampled along the torsional scans, while the weights W_g are all constrained to the same value.

While further details regarding the general procedure can be found in the original papers,[2,3,11] the specific **cproxy**$^-$'s parameterization procedure is outlined in following:

- The atom types for E^{intra}_{QMD-FF} are defined (see Figure S1.a) according only to symmetry and/or chemical equivalence, hence leaving an high degree of flexibility in the choice of the atom labels, which hence allows for a very specific description of the target molecule's internal coordinates and model potentials. It is worth stressing that the same atom types selection is employed in this study for all parameterizations, i.e for both considered states and for each benchmarked functional.

- As far as the stiff $\mathbf{r}^{ric}$ set of ICs is concerned, all possible stretching and bending modes were included in the QMD-FF description. Moreover, several stiff dihedrals defined by quadruplets of heavy atoms were also considered, as those ruling the planarity of the rings or the structure of the cyclo-propyl substituent. Finally, the flexible dihedral (δ, see Figure S1), defined through the quadruplets N_1=C_3-C_4=N_2 and S_1=C_3-C_4=S_2, was also added to the ICs collection.

- As already mentioned, harmonic potentials are employed for all stretching, bending and stiff torsion ICs, while a Fourier-like sum is employed for the flexible dihedral δ (see Figure S1.); the same model functions were employed for both states.

- The usual two-step procedure was adopted: a first JOYCE cycle which fits all harmonic parameters at once and a second cycle, in which the harmonic parameters are fixed ac-

cording to the Frozen Internal Rotation Approximation[2] and the parameters for the flexible dihedral are parameterized against the QM torsional relaxed energy scans. Since the reference QM data are not the same (depending on the employed DFT level of theory and on the considered electronic state), different sets of parameters, assigned to the same collection of atom types/ICs, are expected for each state and tested functional.

S1.2 Intermolecular QMD-FF Parameterization

The point charges driving the electrostatic interaction between the **cproxy**$^-$ solute and the water solvent were also derived from QM data. To include polarization effects due to the solvent on the **cproxy**$^-$'s atoms, the iterative procedure recently developed by some of us in Ref. [10] has been applied as summarized in Figure S2. Concretely, to obtain QM derived polarized point

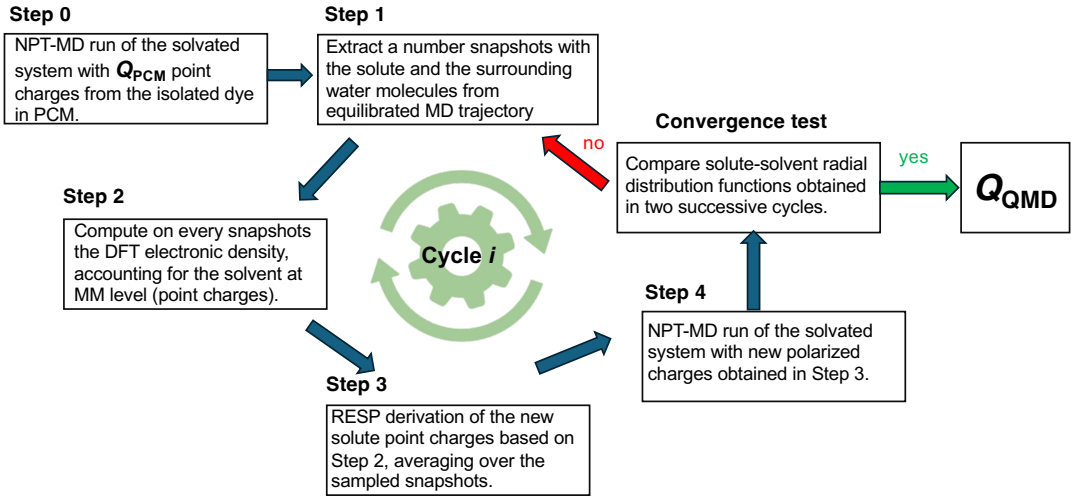

Figure S2: Iterative workflow for Q_{QMD} point charges: Steps 1 to 4 are conducted for each cycle i, until convergence.

charges (Q_{QMD}), the first guesses of point charges are taken from the RESP charges obtained as usual from the electronic density of the dye in PCM[12] solvent (Q_{PCM}). Thereafter, a MD simulation is performed with the resulting point charges (step 0, see Figure S2). A number of snapshots containing the dye and the surrounding H_2O molecules (within 15 Å radius with respect to **cproxy**$^-$'s center of mass) are extracted (step 1, see Figure S2). On each snapshot,

we compute the electronic density taking the polarization effects of the solvent (step 2) using QM/MM level, with the solute at the QM level and the solvent contributing as point charges (MM). We retrieve the new RESP charges (step 3). Finally (step 4) a new MD run is performed with the new charges, ensuring that the solvent re-equilibrates around the **cproxy**$^{-}$. The four steps are then iteratively repeated until convergence, which is evaluated based on the radial distribution functions around the most interacting **cproxy**$^{-}$'s atoms, as displayed in Figures S3 to S4.

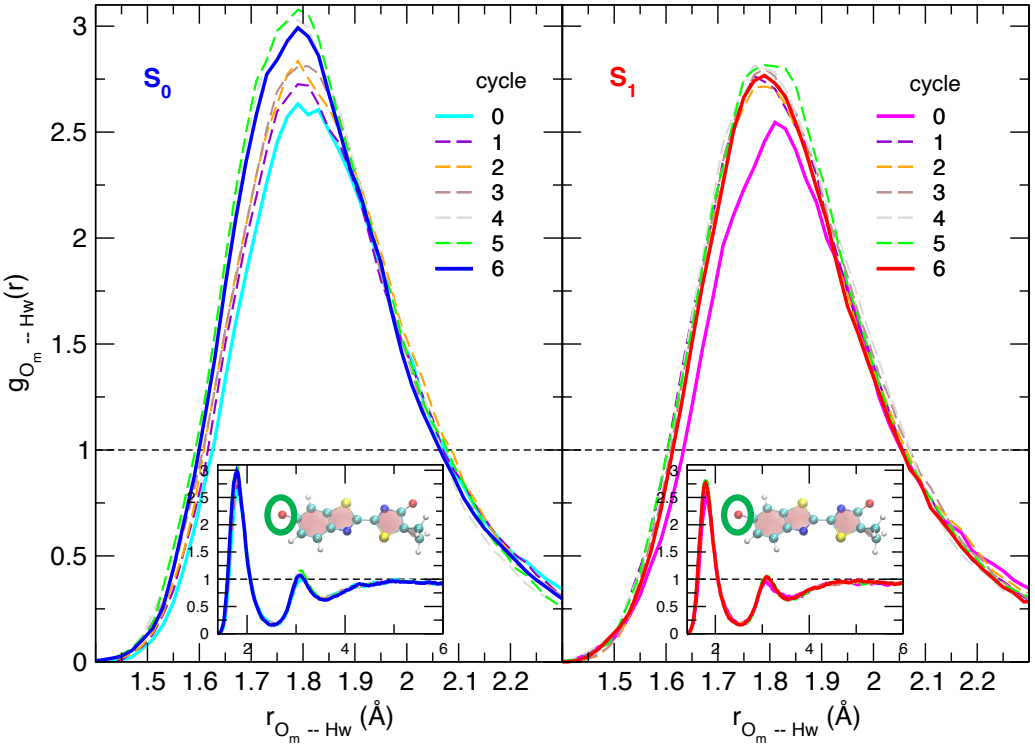

Figure S3: Convergence of the radial distribution function, g_{O_m--Hw}(r), of water hydrogen H$-w$ around the O$_m$ atom (see Figure S1 for definition) of **cproxy**$^{-}$, across the cycles of the Q_{QMD} optimization iterative protocol, carried out for either S_0 (left) and S_1 (right) in case of B3LYP based QMD-FFs.

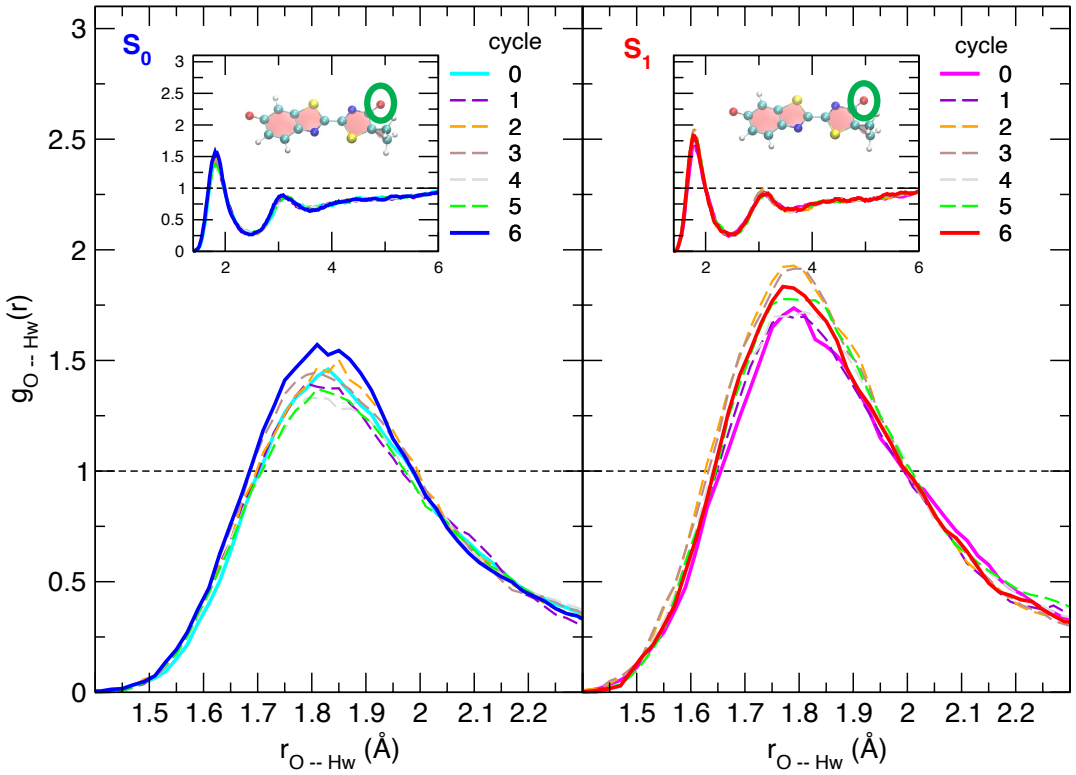

Figure S4: Convergence of the radial distribution function, $g_{O--Hw}(r)$, of water hydrogen H$-w$ around the O atom (see Figure S1 for definition) of **cproxy**$^-$, across the cycles of the Q_{QMD} optimization iterative protocol, carried out for either S_0 (left) and S_1 (right) in case of B3LYP based QMD-FFs.

S2 Intra-molecular QMD-FF validation

To validate the parameterized QMD-FF intra-molecular term, a number of tests were devised and carried out on the isolated chromophore for each considered functional/electronic state, as briefly described in the following.

1. Optimized Structure

The QMD-FF Hessian, $\frac{\partial^2 E^{intra}_{QMD-FF}}{\partial Q_K \partial Q_L}$ is exploited to perform a geometry optimization at MM level on the isolated molecule. The resulting geometry is eventually compared to the QM structure optimized in the same state (S_0 or S_1 state) at the (TD-)DFT level. In all cases, the QM

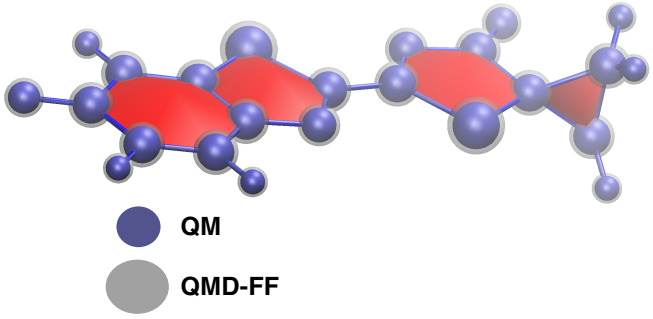

Figure S5: Overlap of the QM (B3LYP, solid blue) and MM (QMD-FF, transparent gray) S_0 optimized geometries of the isolated **cproxy**$^-$ dye. A similar agreement was found for S_1 (not shown).

Table S1: RMSD between QM and MM optimized geometries obtained for all considered functionals and electronic states in terms of bond lengths, bending angle, dihedrals and cartesian (total).

	B3LYP		CAM-B3LYP		ωB97XD	
IC	S_0	S_1	S_0	S_1	S_0	S_1
Bond lengths (Å)	0.00	0.00	0.00	0.00	0.02	0.03
Bending angles (degr)	0.06	0.03	0.05	0.08	0.14	0.18
Dihedrals (degr)	3.30	0.06	0.13	0.18	0.05	0.06
Total (Å)	0.09	0.01	0.02	0.03	0.01	0.06

and QMD-FF optimizations yield similar structures: as an example, Figure S5 compares the optimized geometries obtained at QM (B3LYP) and MM level for the S_0 state. It is evident that the QM and MM structures nicely overlap and no geometrical distortions are encountered. This

visual analysis is confirmed by looking at Table S1, where the standard deviation between QM and MM optimized structures is reported for all states and functionals, in terms of bond lengths, angles, dihedrals and with respect to the molecular normal modes.

2. Vibrational Modes

Exploiting the QMD-FF Hessian matrix, the MM normal modes can be computed together with their associated vibrational frequencies and the results eventually compared to the QM parent data, employed in the JOYCE procedure. The comparison is displayed in Figure S6 for

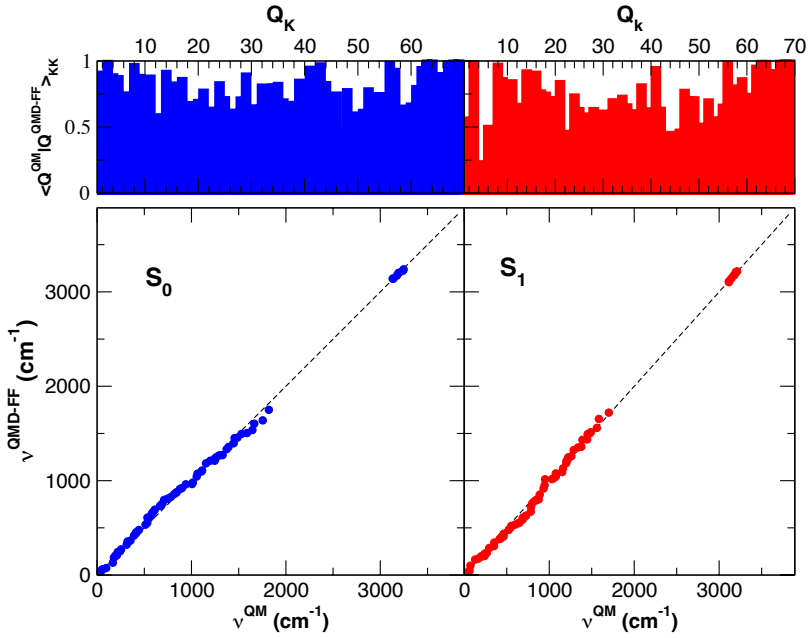

Figure S6: Top panels: overlap of QM and QMD-FF normal modes for B3LYP functional, computed as $< Q_K^{QM} | Q_K^{QMD-FF} >$ for each Q_K mode. Bottom panels: correlation plot between QM and QMD-FF vibrational frequencies for B3LYP functional. Left (blue) and right (red) bars and symbols refer to the ground and first excited state, respectively. Similar results (not shown) were obtained for all considered functionals.

both states, both concerning the QM/MM normal mode overlap ($< Q^{QM} | Q^{QMD-FF} >_{KK}$, top panels) and the QM/MM frequency correlation (ν^{QM} vs ν^{QMD-FF}, bottom panels).

The final validation test that has been performed concerns the internal molecular flexibility, and the capability of the QMD-FF description to accurately describe the possible large amplitude oscillations that the δ dihedral could experience at room temperature. In the main text, Figures 3 and 4 compares the relaxed torsional energy scans carried out for the flexible dihedral

at QM or MM level, for both electronic states with all considered functionals.

S3 LVC model parametrization and Quantum dynamics

Here are discussion on Linear Vibronic Coupling model parametrization and Quantum dynamics.

S3.1 Vibronic Model Hamiltonian

We adopt ground state dimensionless normal coordinates $\mathbf{q}$ and associated momenta $\mathbf{p}$ and write down a LVC Hamiltonian for a set of coupled electronic diabatic states d_η:

$$\mathbf{H} = \sum_\eta \Big(K + V^{dia}_{\eta\eta}(\mathbf{q})\Big) |d_\eta\rangle \langle d_\eta| + \sum_{\eta,\zeta>\eta} V^{dia}_{\eta\zeta}(\mathbf{q}) \Big(|d_\eta\rangle \langle d_\zeta| + |d_\zeta\rangle \langle d_\eta| \Big) \quad (1)$$

The kinetic (K) and potential (V) energy terms read

$$K = \frac{1}{2}\mathbf{p}^T \boldsymbol{\Omega} \mathbf{p} \quad (2)$$

$$V^{dia}_{\eta\eta}(\mathbf{q}) = E^0_\eta + \boldsymbol{\lambda}^T_{\eta\eta}\mathbf{q} + \frac{1}{2}\mathbf{q}^T \boldsymbol{\Omega} \mathbf{q} \quad (3)$$

$$V^{dia}_{\eta\zeta}(\mathbf{q}) = E^0_{\eta\zeta} + \boldsymbol{\lambda}^T_{\eta\zeta}\mathbf{q}. \quad (4)$$

Here $\boldsymbol{\Omega}$ is the diagonal matrix of the vibrational frequencies of the ground state g, E^0_η the η-th excited-state energy at the g equilibrium geometry, $\boldsymbol{\lambda}_{\eta\eta}$ is the energy gradient of state η and $\boldsymbol{\lambda}_{\eta\zeta}$ is the gradient of the inter-state coupling $V^{dia}_{\eta\zeta}(\mathbf{q})$. The diabatic states are built exploiting a maximum-overlap diabatization technique. In practice at a given reference geometry they are defined to be identical to the adiabatic states considered as reference states. Afterward, the molecular geometry is modified with positive and negative displacements along each normal mode and the diabatic states are computed through the rotation of the adiabatic states that make them as similar as possible to the reference states. Applying such rotation to the adiabatic energies one gets the diabatic Hamiltonian.[13] Finally $\boldsymbol{\lambda}_{\eta\eta}$ and $\boldsymbol{\lambda}_{\eta\zeta}$ values can be straightforwardly calculated from the numerical derivative of the terms of the diabatic Hamiltonian.[14] Setting to zero the diabatic couplings $\boldsymbol{\lambda}_{\eta\zeta} = 0$ the non-adiabatic LVC model collapses into the VG adiabatic model.

S3.2 LVC parametrization

We parameterized the LVC Hamiltonian in Eq 1 in gas phase taking as reference geometry the ground state equilibrium geometry and considering the first 6 electronic adiabatic states as reference states. In principle one can generalize our mixed quantum classical approach Ad-MD|gVG so to account both for the solvent effects and also for inter-state couplings by substituting the VG adiabatic model with an LVC non-adiabatic model, thus getting what we named a Ad-MD|gLVC approach.[15] In principle the application of method would require a fully parameterization of the LVC model at each snapshot of the MD. Such a procedure would be extremely expensive from the computational point of view. Therefore in order to have an approximate estimate of the impact on the spectrum of the combined effect of nonadiabatic couplings and solvent fluctuation we made a zero-order approximation and we assumed that the only parameters of the LVC model that vary with the snapshot are the vertical energies E_η^0. We further assumed that at each snapshot the values E_η^0 can be assimilated with the vertical energies of the first 6 states. The accuracy of these approximations can be questioned but since the outcome of these computation suggest that the Ad-MD|gLVC spectrum is very similar to the Ad-MD|gVG one and therefore the impact of nonadiabatic couplings is minimal we decided not to refine further the model.

S3.3 Quantum dynamics

The absorption spectrum for each snapshot α was computed within a time-dependent framework:

$$\varepsilon_\alpha(\omega) = \omega \sum_{\zeta\eta} \int_{-\infty}^{\infty} dt e^{i\omega t - \Gamma t^2} \langle \mathbf{0}; d_\zeta | \boldsymbol{\mu}_{g\zeta} e^{-i\mathbf{H}_\alpha t/\hbar} \boldsymbol{\mu}_{\eta g} | d_\eta; \mathbf{0} \rangle \tag{5}$$

where ω is the frequency, $\boldsymbol{\mu}_{gb}$ is the electric transition dipole moments between the ground state g and the excited state $b = \eta, \zeta$ and we introduced a Gaussian damping in time that corresponds to a Gaussian broadening in the frequency domain.

Since for the LVC Hamiltonian there is no analytical expression for the correlation functions in brackets, they were calculated numerically by propagating multidimensional nuclear

wavepackets on the coupled diabatic potential energy surfaces (PESs) adopting the Multi-Layer Multi-Configurational Time-Dependent Hartree (ML-MCTDH) method as implemented in the Quantics code.[16]

The final absorption spectrum was obtained as an average of the spectra $\varepsilon_\alpha(\omega)$ computed for a subset of the 100 different snapshots used for Ad-MD|gVG, and namely $\alpha = 5(i-1)+1$ with $i = 1,20$.

S4 Dye's internal structure and dynamics

Considering the very similar performances achieved with all considered FFs in terms of fast vibrations in a local harmonic approximation (LHA), to investigate the effect of different QMD-FF on the conformational dynamics of the solvated **cproxy**$^-$ dye, preliminary MD simulations were carried out on a system composed of one dye and $\sim$ 100 water molecules. For each FF, 10 ns trajectories were collected after equilibration at 300 K and 1 atm, and employed to monitor time-behaviour and distributions of the most flexible **cproxy**$^-$'s coordinates, i.e. the δ dihedral, where the differences between the "pure" TD-DFT and CASPT2 parameterization strategies should show larger differences. Figure S7 shows the results achieved using the CAM-B3LYP

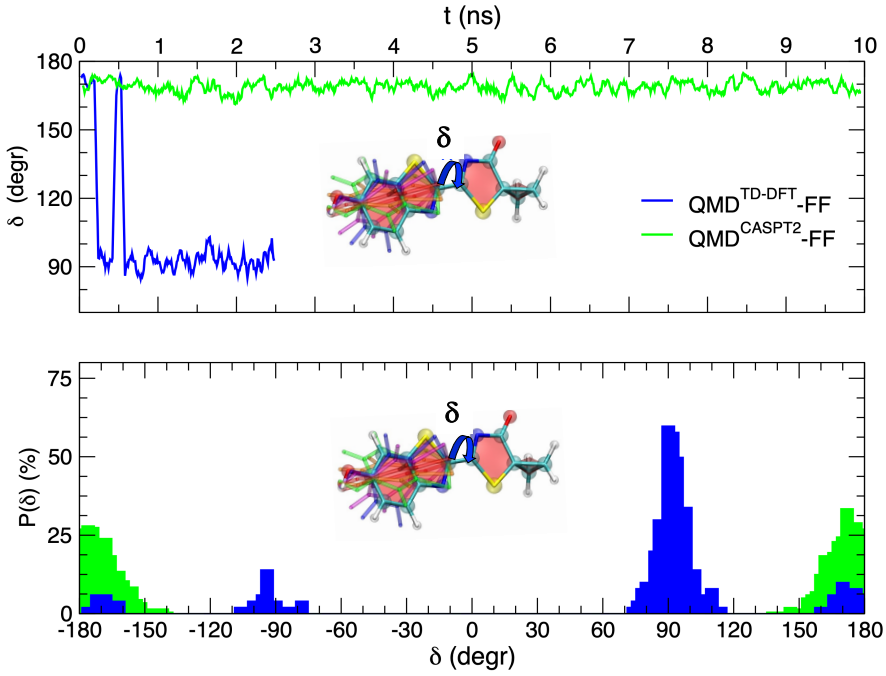

Figure S7: Conformational dynamics of the hydrated **cproxy**$^-$ in its excited state computed with the QMD-FF either solely parameterized on TD-DFT data (CAM-B3LYP, blue) or corrected (green) with the CASPT2 torsional profiles (see Figure 4 in the main text). Top: time behaviour of the δ angle, see insets for definition. Bottom: distribution achieved along the NPT dynamics with the two considered S_1 QMD-FFs.

functional and the two QMD-FF built on such description. Similar results (not shown) were delivered when employing other functionals.

S5 Solvation structure

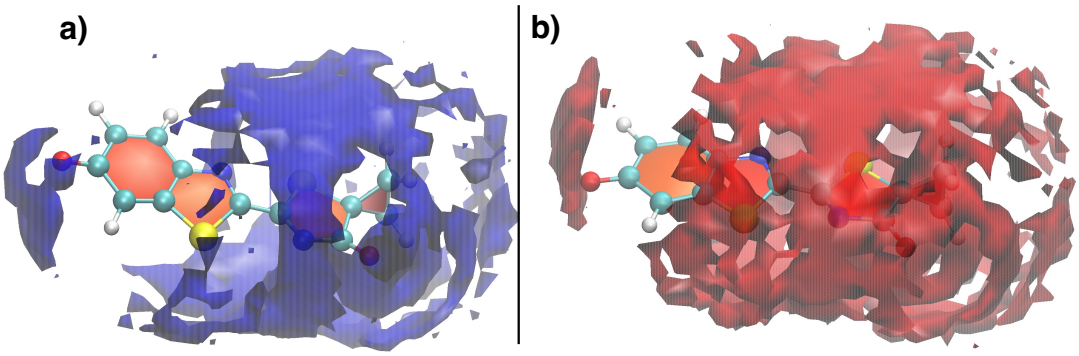

Figure S8: Spatial distribution functions of the water proton (Hw) with respect to **cproxy**$^-$'s five-membered thiazolone hetero-cycle. All functions are obtained from the NPT-MD runs carried out with the QMD-FF parameterized for either a) S_0 (blue) or b) S_1 (red).

S6 Spectroscopy

S6.1 Effect of the number of states on the absorption spectrum

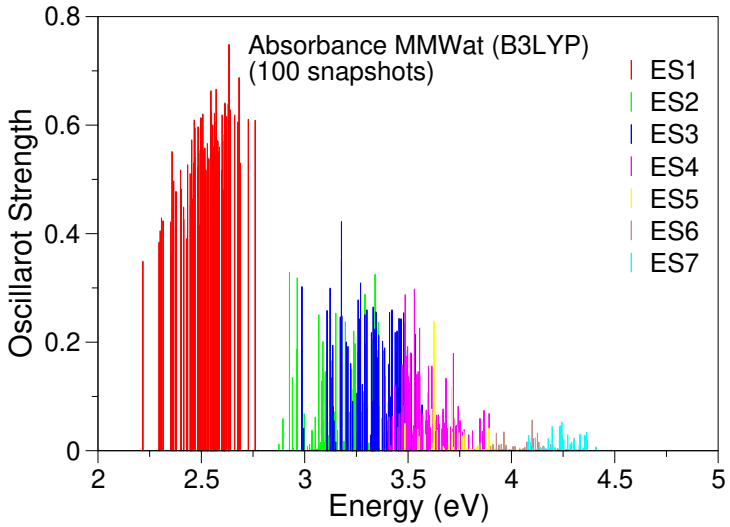

Figure S9: Possible contribution of different excited states (ESs) in the simulation of absorption spectra of the **cproxy**$^-$molecule in a water box. Computations were performed at the B3LYP/6-311G(2d,p) level with the first solvent shell at MM and the outer layer at PC. Results for the vertical excitation of the first 7 excited states over 100 snapshots from an MD with Q_{QMD} charges. It is shown that the vertical excitation for ES 7 is never lower than 4 eV. Analysis of the the AdMD|gVG spectrum in Figure 10 computed considering 6 ESs and its comparison with experiment indicates that the second band is practically over at 4 eV and therefore the contribution of state 7 or higher might only be relevant for the very blue-tail of the second band and for additional higher lying bands.

S6.2 Effect of the number of selected shapshots in the AdMD|gVG spectra

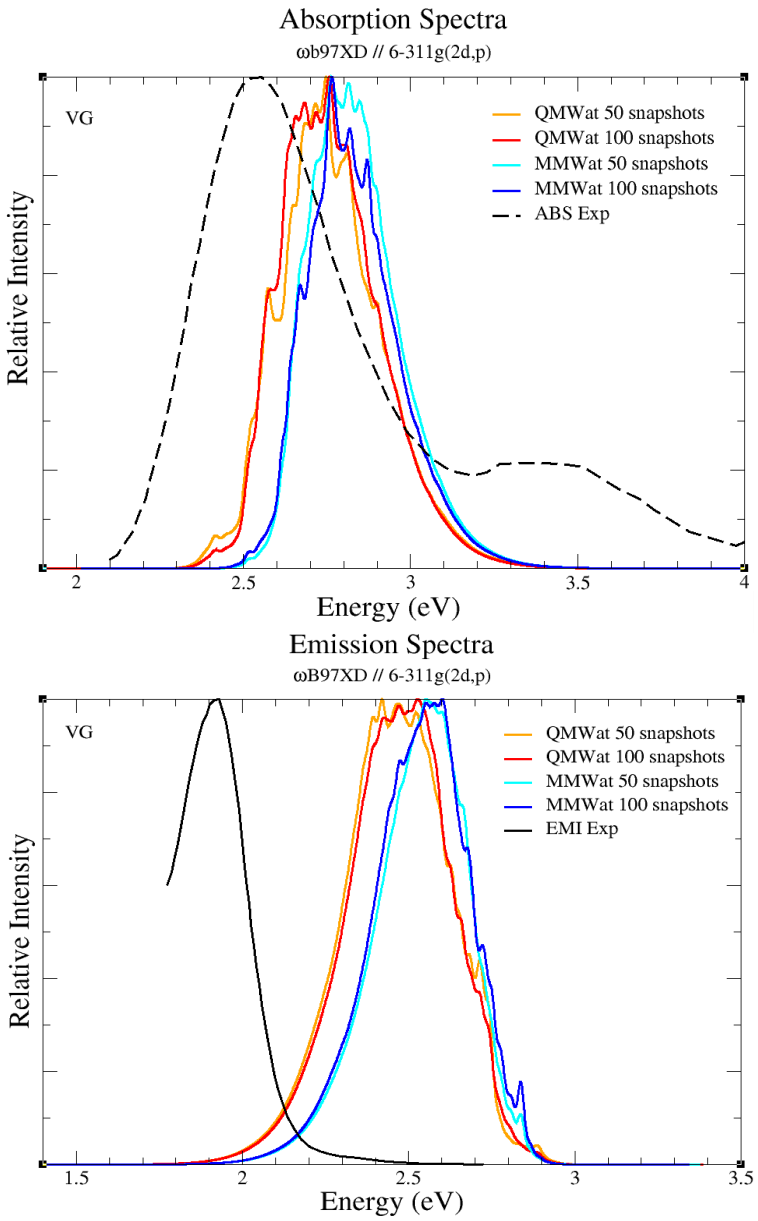

Figure S10: Test on the convergence of absorption and emission spectra obtained with the AdMD|gVG considering either 50 or 100 snapshots. Computations with the ωB97XD functional and the QMwat model after an MD performed with the Q_{QMD} charges. Differences of the spectra obtained with 50 and 100 snapshots are minimal. The experimental spectra were taken from reference.[17] Copyright 2018 American Chemical Society.

S6.3 Effect of the basis set

In this section we investigate the effect of the introduction of diffuse functions in our basis set comparing results adopted with the basis set 6-311G(2d,p) adopted in all our computations and with the 6-311+G(2d,p) basis set.

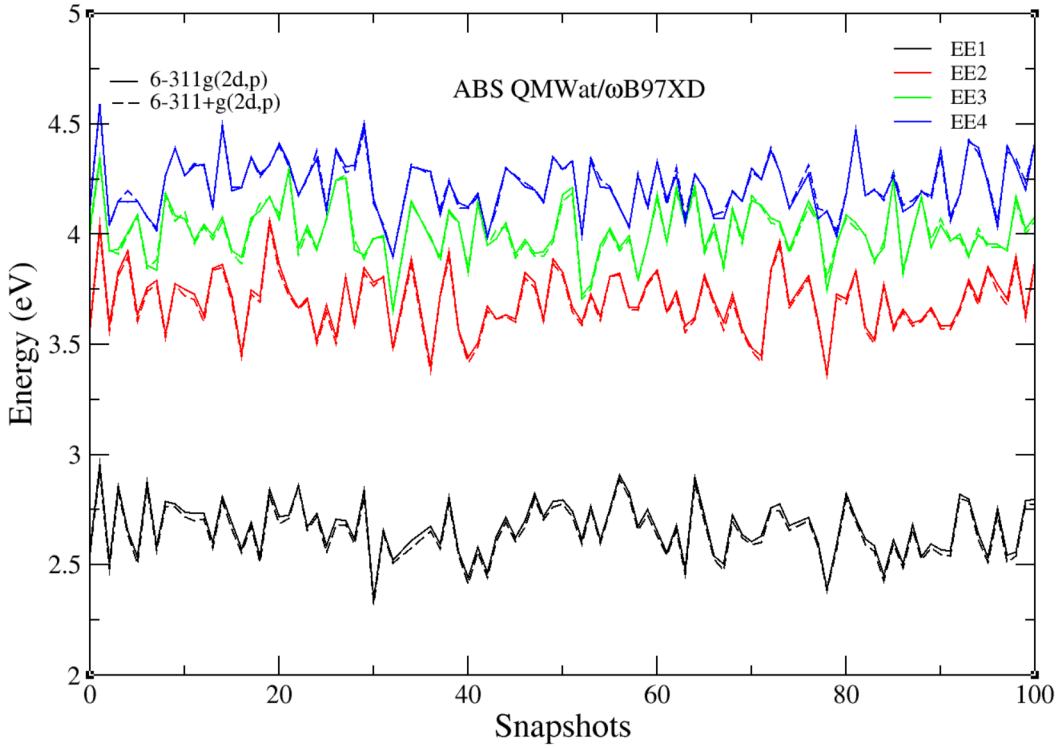

Figure S11: Test on the effect of the inclusion of a set of diffuse functions on the vertical excitation energies of the first 4 excited states at the 100 snapshots adopted for the computation of AdMD|gVG absorption spectrum with ωB97XD functional and the QMwat model after an MD performed with the Q_{QMD} charges. Results for the 6-311G(2d,p) basis set (solid line) adopted in all our computations and with the 6-311+G(2d,p) basis set (dashed lines) are practically indistinguishable.

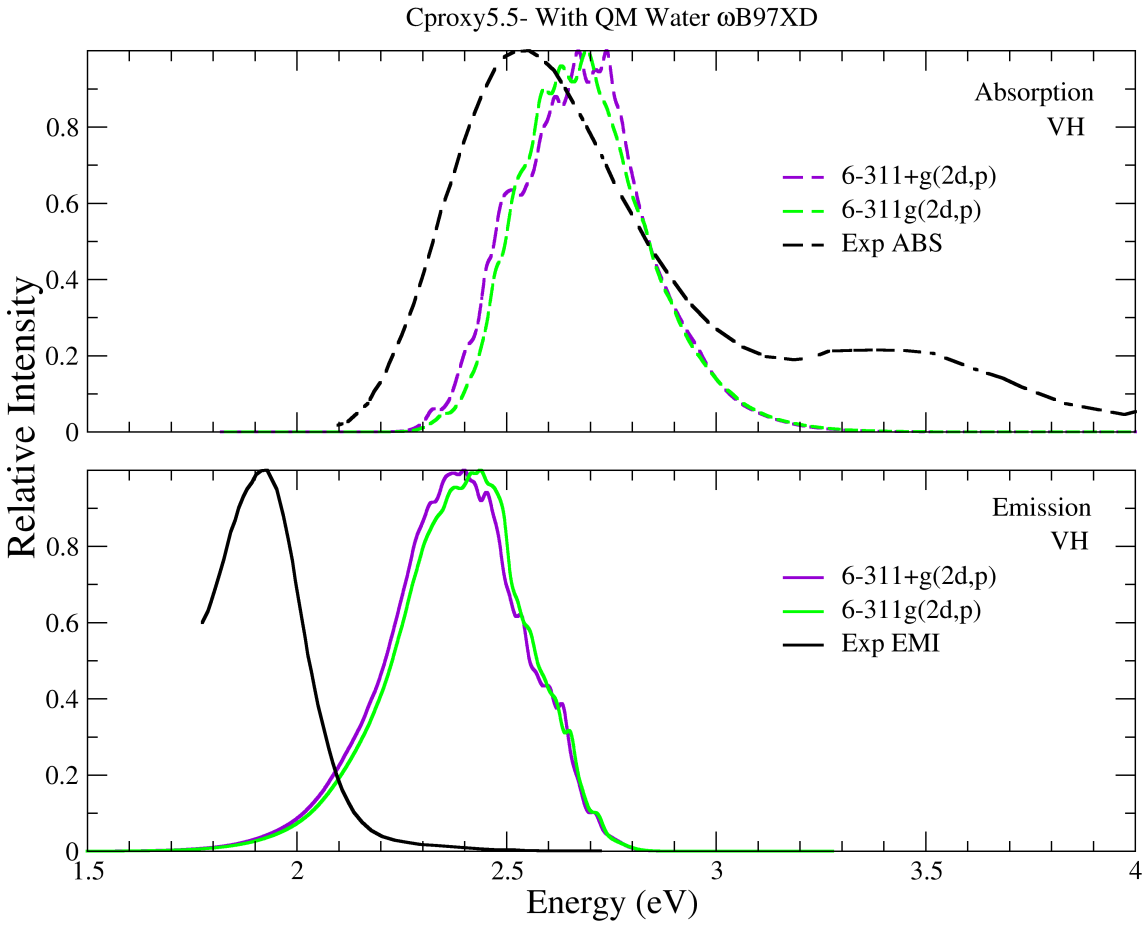

Figure S12: Test on the effect of the inclusion of a set of diffuse functions on the fisrst band of the absorption spectrum and on the emission spectrum computed with the AdMD|gVG method in combination with ωB97XD functional and the QMwat model after an MD performed with the Q_{QMD} charges. Resutls obtained with the 6-311+G(2d,p) basis set (green) are only marginally different from those obtained with the 6-311G(2d,p) basis set (purple) adopted in all our computations. The experimental spectra were taken from reference.[17] Copyright 2018 American Chemical Society.

S6.4 Effect of outer solvent shells

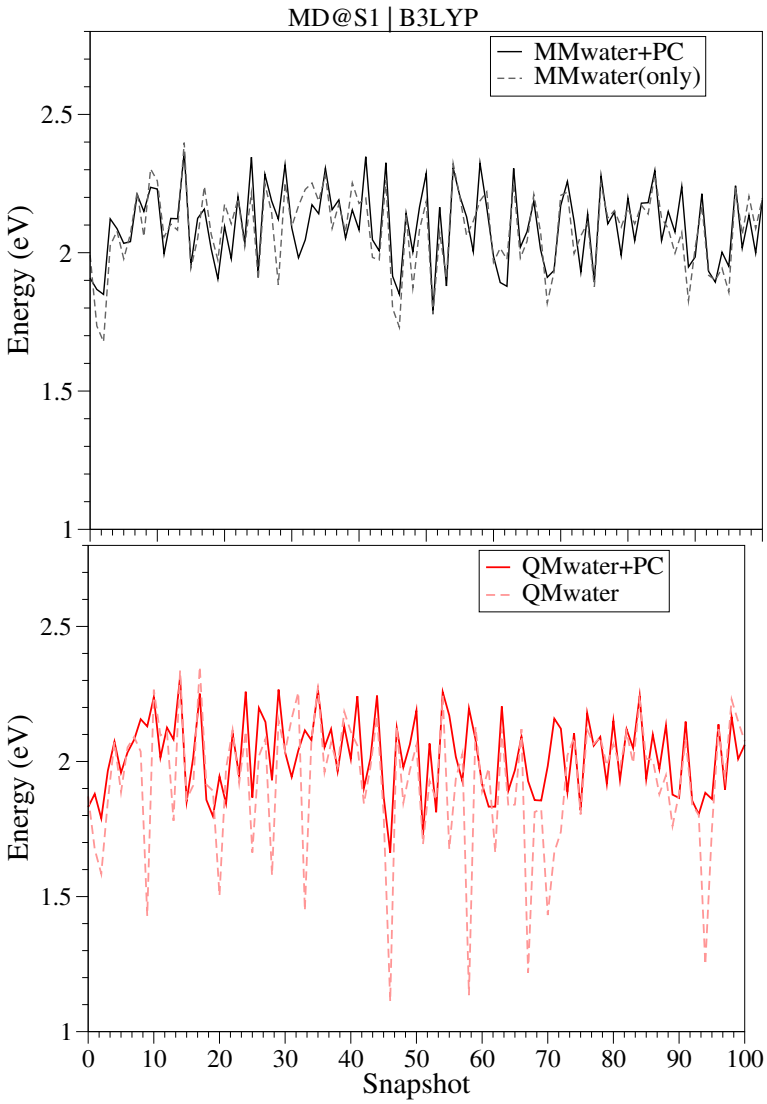

Figure S13: Vertical energies computed over the trajectory conducted in S_1, including the first solvent shell at MM (upper panel) or QM (bottom panel) level. Outer solvent layers are either kept (within a radius of 15Å) as point charges (+PC) (plain lines) or ignored in the calculation (dashed lines). The main difference arise in the case of the first solvent layer treated at QM level, which shows well known spurious charge transfer states involving solvent molecules.[18] Such spurious states are "corrected" when point charges are included.

S6.5 Effect of the phenomenological broadening

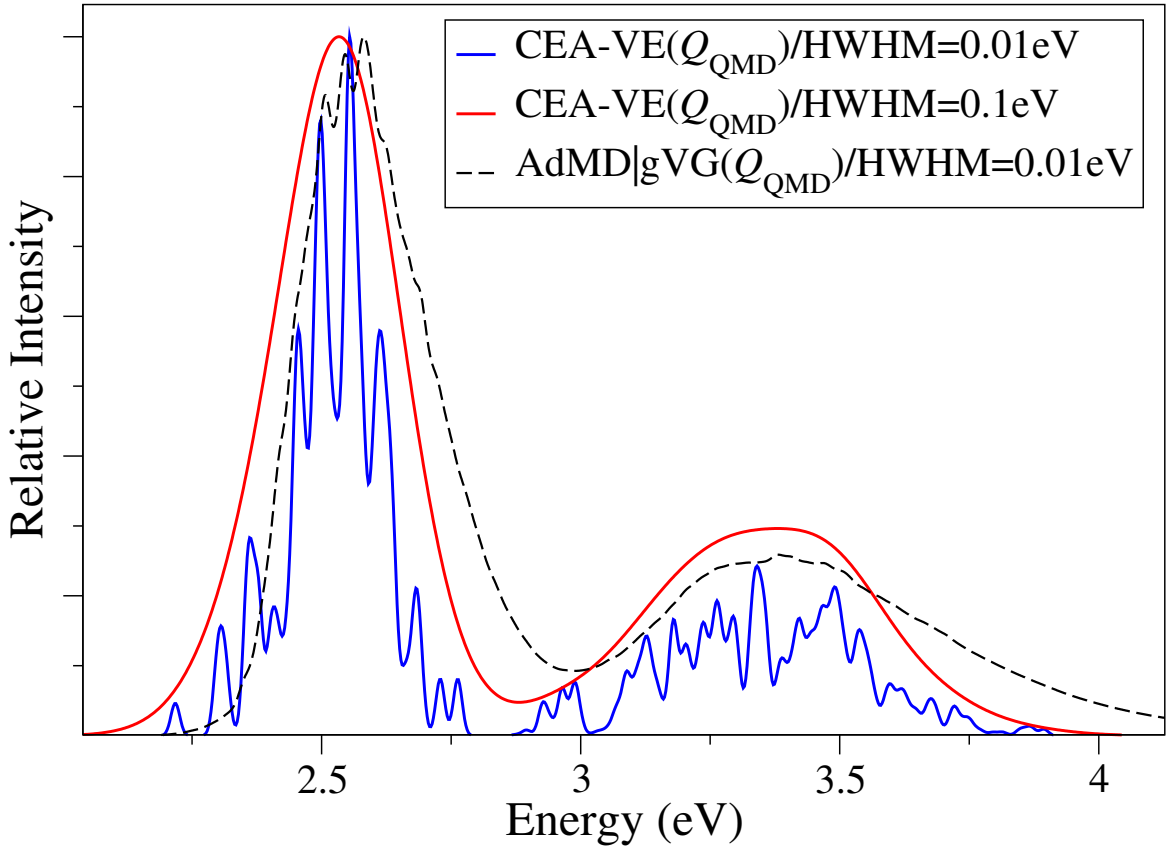

Figure S14: Absorption spectrum simulated with the B3LYP functional employing the CEA-VE method and adopting a Gaussian broadening with either a small HWHM (0.01 eV) or the arbitrary value chosen in this work (0.1 eV). For comparison, the AdMD|gVG spectrum computed with a HWHM=0.01 eV is also included.

S6.6 Single point computations with CASPT2 at the S_0 and S_1 optimized geometries

We computed the vertical transition energies with Single state (SS) CASPT2 and Multistate (MS) CASPT2 at the S_0 and S_1 geometries optimized with DFT and different functionals. Like for the energy profiles discussed in the main text we used a CASSCF(10,10) in combination with the 6-311G(d,p) basis set, an imaginary level shift of 0.2 au and an IPEA equal to zero.

Table S2: Vertical transition energies (eV) in absorption and emission computed with TD-DFT, Single state (SS) CASPT2 and Multistate (MS) CASPT2 in gas phase.

S_0 optimized geometry B3LYP		
B3LYP	SS CASPT2	MS CASPT2
2.58	2.12	2.20
S_1 optimized geometry B3LYP		
B3LYP	SS CASPT2	MS CASPT2
2.26	1.88	1.97
S_0 optimized geometry CAM-B3LYP		
CAM-B3LYP	SS CASPT2	MS CASPT2
2.74	2.15	2.22
S_1 optimized geometry CAM-B3LYP		
CAM-B3LYP	SS CASPT2	MS CASPT2
2.56	1.96	2.06
S_0 optimized geometry ωB97-XD		
ωB97-XD	SS CASPT2	MS CASPT2
2.73	2.14	2.21
S_1 optimized geometry ωB97-XD		
ωB97-XD	SS CASPT2	MS CASPT2
2.56	1.97	2.07

S6.7 Spectral shifts adopted for emission

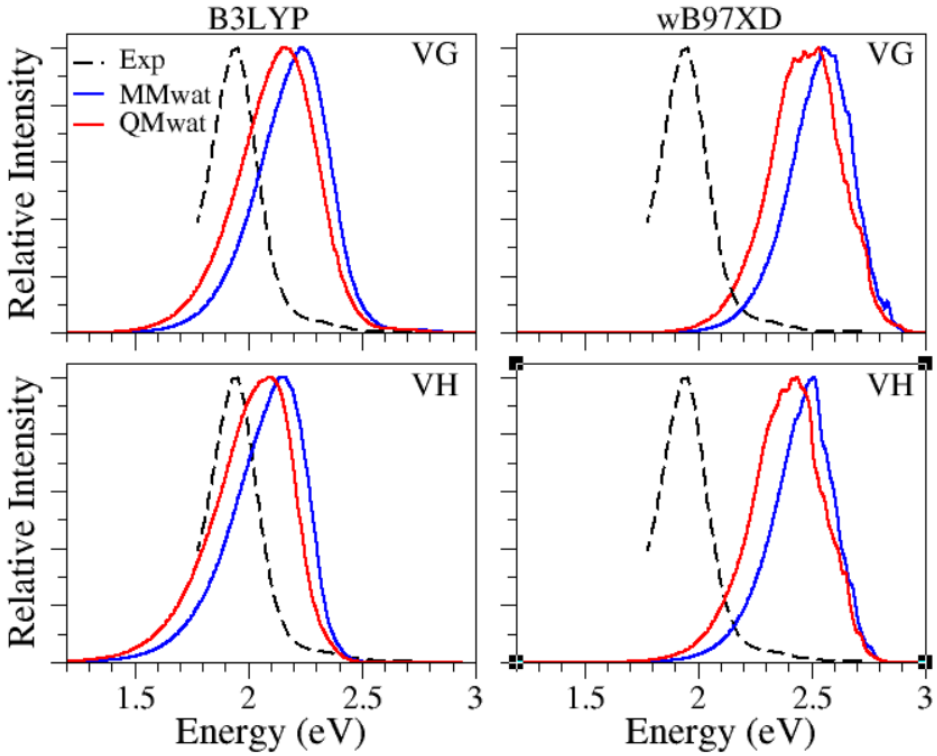

Figure S15: The un-shifted emission spectra computed with B3LYP (left) and ωB97XD (right) and with Ad-MD|gVG (top) or Ad-MD|gVH (bottom) mixed quantum classical approaches, and two different QM/MM models for TD-DFT in which the first sphere of solvent molecules is treated at MM level (MMwat) (blue lines) or at QM level (QMwat) (red lines). The shifts applied to obtain the shifted spectra of the main manuscript are given in table S3. The experimental spectra were taken from reference.[17] Copyright 2018 American Chemical Society.

Table S3: Energy shifts 8eV) added to the data of Figure S15 to superimpose the emission spectra for Figure 9 of main manuscript.

Emission							
B3LYP				ωB97XD			
VG		VH		VG		VH	
MMWat	QMWat	MMWat	QMWat	MMWat	QMWat	MMWat	QMWat
x-0.30	x-0.23	x-0.20	x-0.14	x-0.60	x-0.56	x-0.56	x-0.46

S6.8 Spectral shifts adopted for absorption

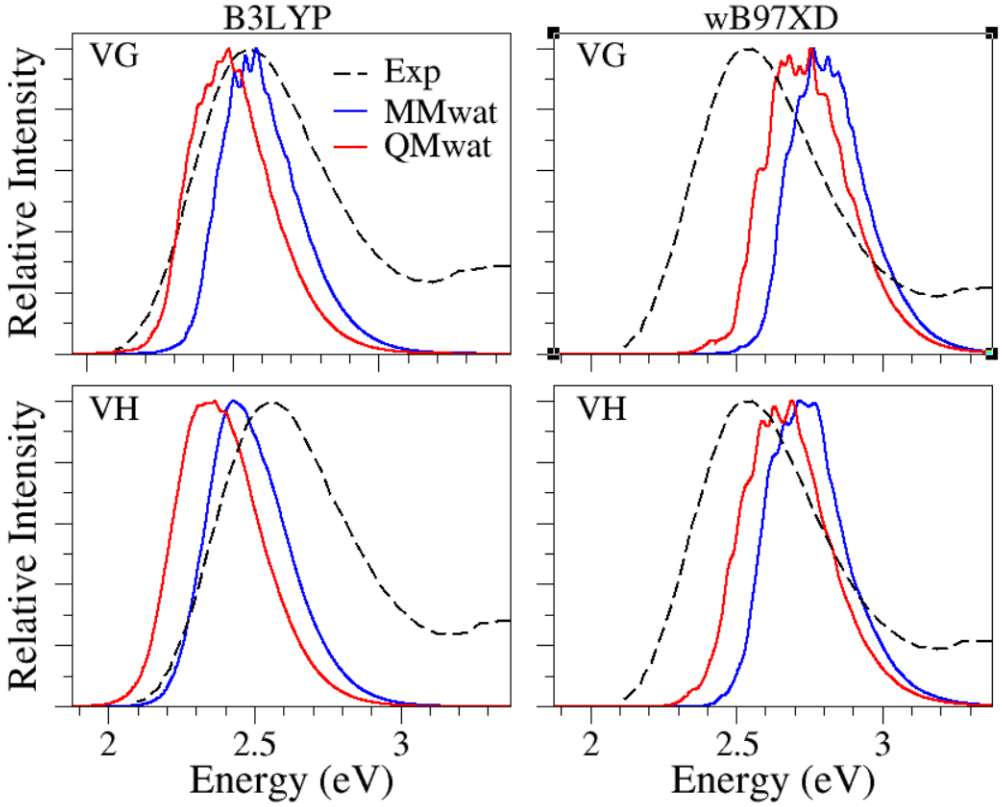

Figure S16: The un-shifted absorption spectra computed with B3LYP (left) and ωB97XD (right) and with Ad-MD|gVG (top) or Ad-MD|gVH (bottom) mixed quantum classical approaches, and two different QM/MM models for TD-DFT in which the first sphere of solvent molecules is treated at MM level (MMwat) (blue lines) or at QM level (QMwat) (red lines). The shifts applied to obtain the shifted spectra of the main manuscript are given in the table S4 below. The experimental spectra were taken from reference.[17] Copyright 2018 American Chemical Society.

Table S4: Energy shifts (eV) added to the data to superimpose the absorption spectra of figure S16

Absorption							
B3LYP				ωB97XD			
VG		VH		VG		VH	
MMWat	QMWat	MMWat	QMWat	MMWat	QMWat	MMWat	QMWat
x+0.00	x+0.07	x+0.14	x+0.23	x-0.23	x-0.17	x-0.18	x-0.10

S6.9 Vibronic spectra at MD frames

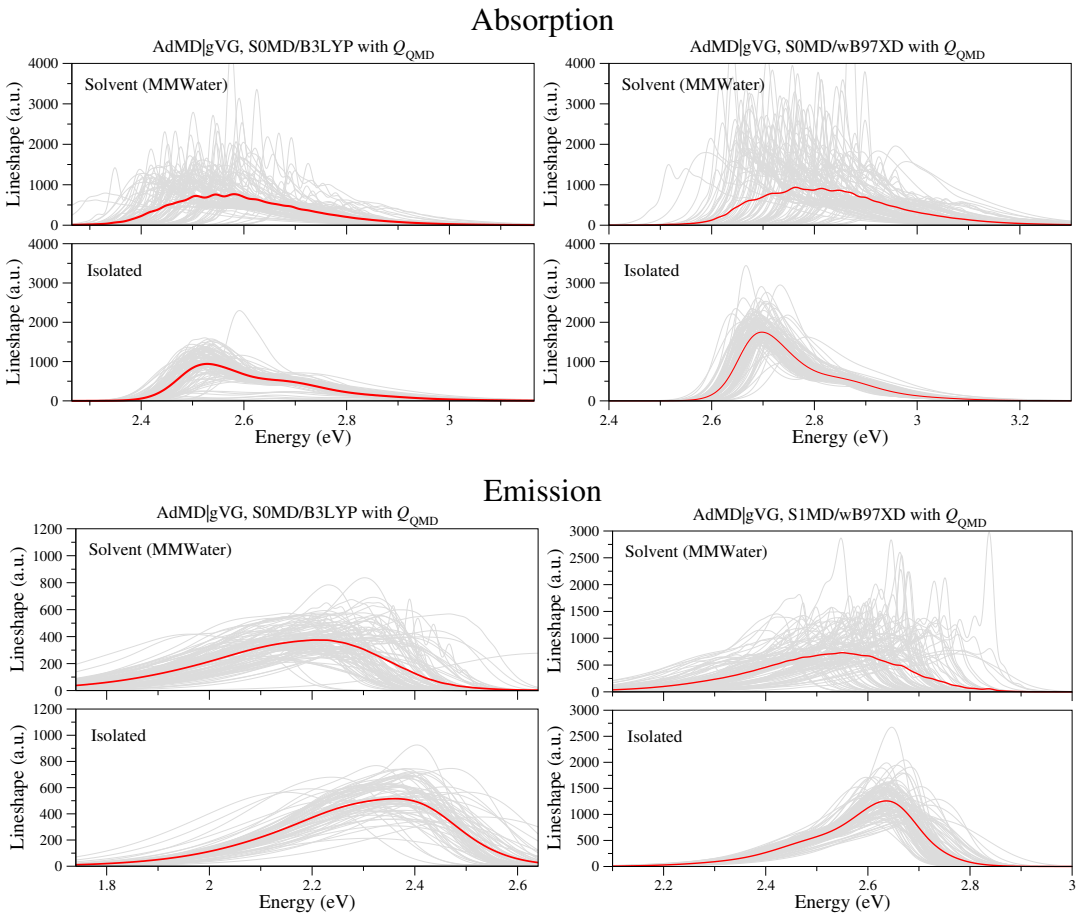

Figure S17: Absorption and emission spectra computed with AdMD|gVG spectra using the protocol indicated in the main text (i.e., considering solvent molecules around 4 Å in the MM layer (upper panels) or eliminating all solvent molecules from the snapshot when computing energies, gradients and Hessians (isolated molecules, lower panels). Spectra computed with both B3LYP (left) and ωB97XD (right) functionals. The results indicate that the main source of broadening is the effect of the solvent, as the spectral width of the average spectrum is reduced when the solvent is eliminated.

S6.10 Effect of the inter-state couplings

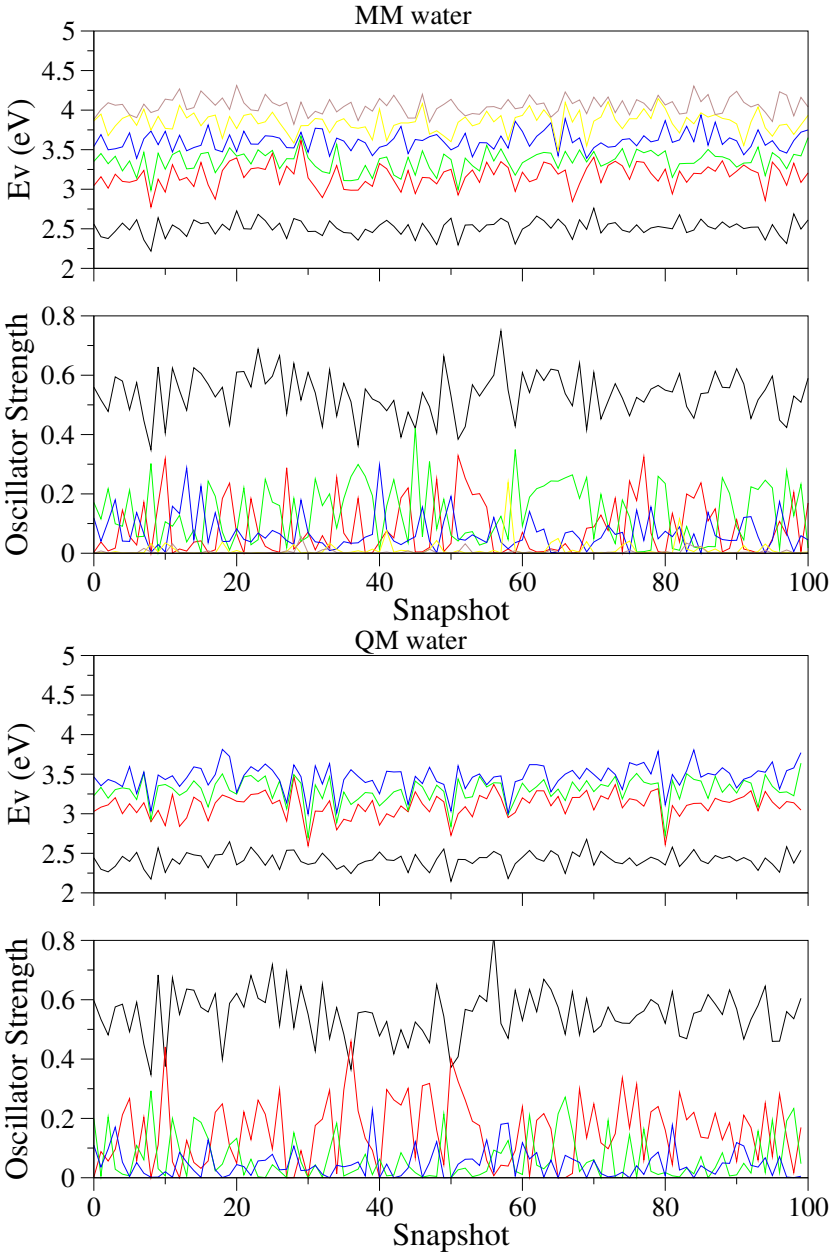

Figure S18: Vertical energies and oscillator strengths for the lowest-lying excited states, from S_0 to S_1 in black, S_2 in red, S_3 in green, S_4 in blue, S_5 in yellow, and S_6 in pink, computed along the MD trajectory carried out with Q_{QMD} charges. The values are computed at the TD-DFT level with the B3LYP functional including the water molecules at 4 Å either at MM level (upper panels) or QM level (lower panels).

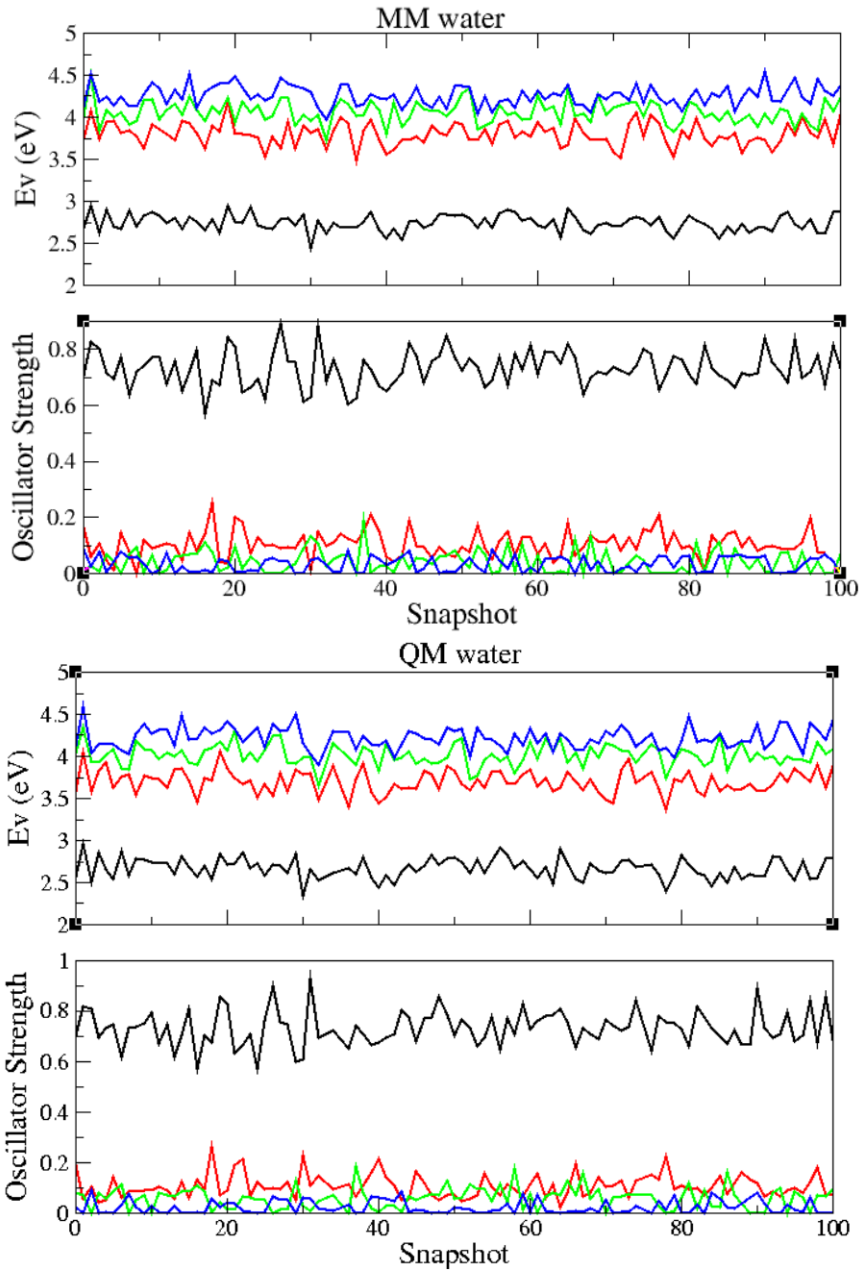

Figure S19: Vertical energies and oscillator strengths for the lowest-lying excited states, from S_0 to S_1 in black, S_2 in red, S_3 in green and S_4 in blue, computed along the MD trajectory carried out with Q_{QMD} charges. The values are computed at TD-DFT level with ωB97XD funtional including the water molecules at 4 Å either at MM level (upper panels) or QM level (lower panels).

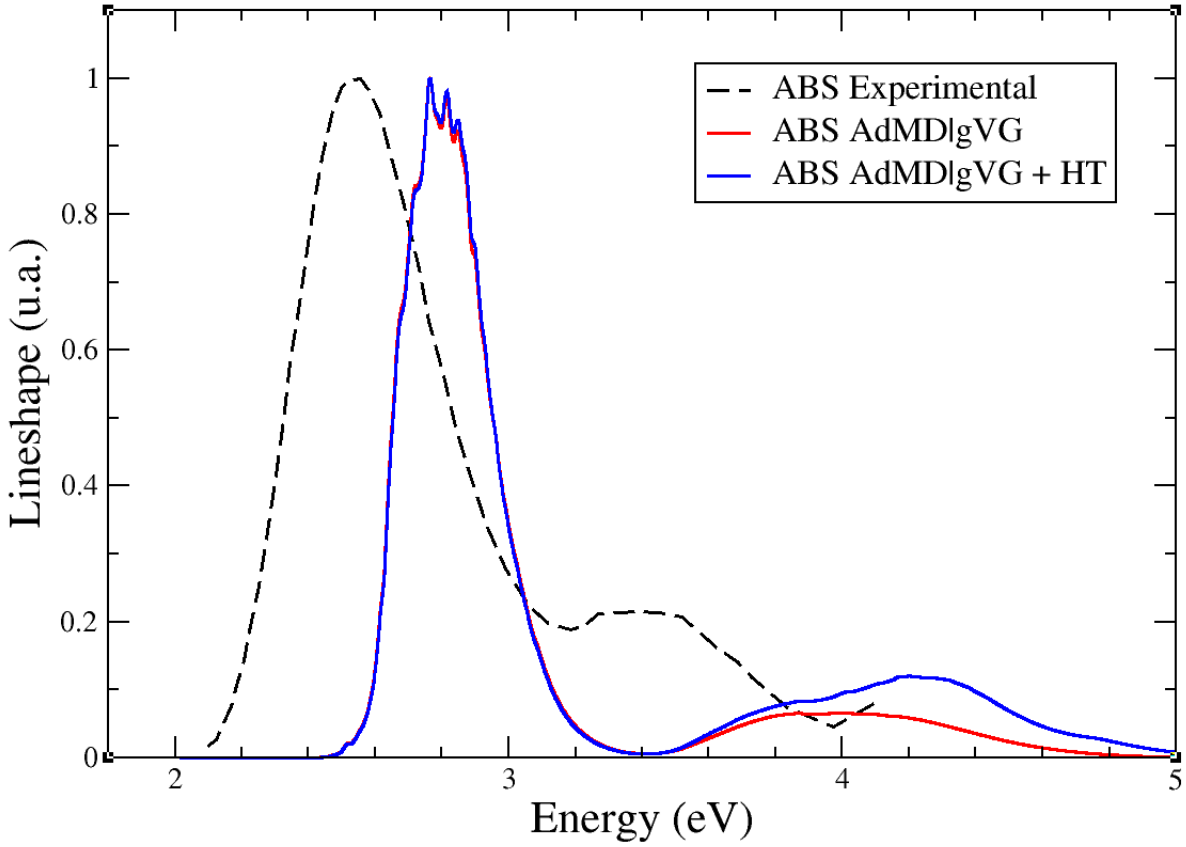

Figure S20: The experimental absorption spectrum (dashed black) compared with the un-shifted absorption spectra computed using the ωB97XD functional. The spectra were obtained through a mixed quantum-classical Ad-MD|gVG approach (red) and the Ad-MD|gVG + Herzberg-Teller (HT) correction (blue). The experimental spectrum was taken from reference.[17] Copyright 2018 American Chemical Society.

S6.11 Distribution of vertical energies

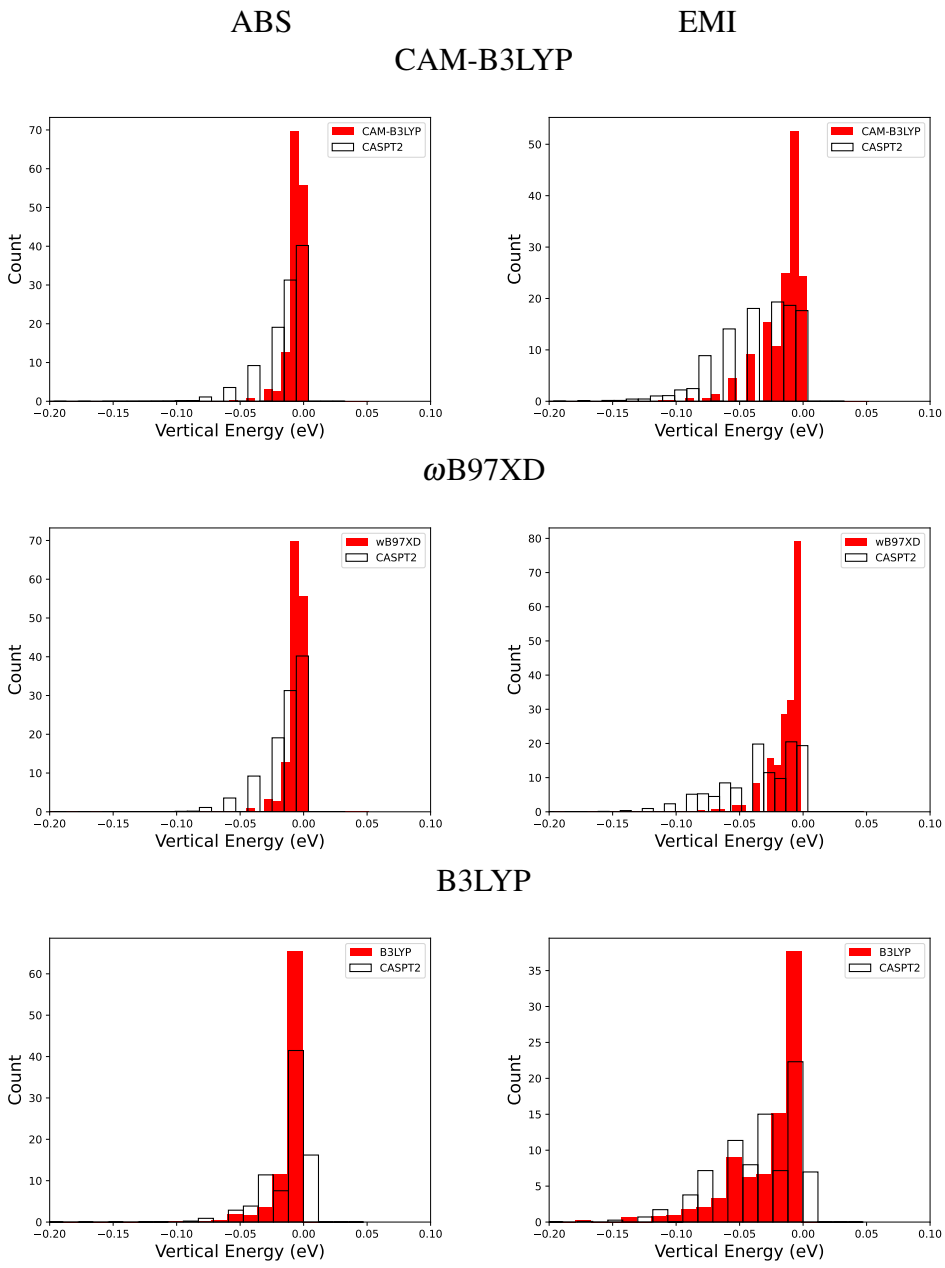

Figure S21: Distribution of vertical energies computed from the relaxed scans along the torsional degree of freedom δ in Figs. 3 and 4 in the main text. The vertical energies are computed either among the S_0 and S_1 potential energy curves corresponding to each functional, or using the functional for S_0 and CASPT2 results for S_1. The Boltzmann weights used to derive the distributions are computed from the S_0 curve computed with CAM-B3LYP (for absorption) and the S_1 curve computed with CASPT2 (for emission).

In Figure S21 we report the distribution of vertical energies along the torsional degree of freedom, computed from the relaxed scans in Figs. 3 and 4 in the main text. The distributions are computed applying the Boltzmann weights at each grid point of the scan, which are taken from the profile used to parameterize the FF used to run the MD simulations (DFT for S_0 and CASPT2 for S_1), while the transition energies are computed from DFT to either TDDFT values or CASPT2 ones. Such a strategy, already applied to analyze the contribution of flexible coordinates to the spectrum for other dyes, implies a classical treatment of nuclear degrees of freedom, which is reasonable for low-frequency motions.[19] We note that instead of directly taking the grid points from the original energy scans (with a step of 15°), we first performed an interpolation and subsequently take a step of 3.6°. Moreover, in order to focus on the broadening, not on the position of the bands, we report the vertical energies subtracting the adiabatic energy (namely, we applied the same origin of energies reported in Figs. 3 and 4, in the main text). The distribution of vertical energies depicted in this figure, provides an estimate of broadening induced by the nuclear motion along this degree of freedom. Namely, as shown in the plots, in the case of absorption, using CASPT2 to evaluate the vertical energies would have resulted in a broader spectrum, compared to TDDFT, which would have lied closer to the experiment. In the case of absorption, the induced broadening would also be generally larger with CASPT2, except in the case of B3LYP, where it is expected to be similar to that deliver by CASPT2.

References

[1] Cacelli, I.; Cerezo, J.; De Mitri, N.; Prampolini, G.; JOYCE2.10, a Fortran 77 code for intra-molecular force field parameterization. , available free of charge at http://www.iccom.cnr.it/en/joyce-2/, last consulted September 2022.

[2] Cacelli, I.; Prampolini, G. Parametrization and Validation of Intramolecular Force Fields Derived from DFT Calculations *J. Chem. Theory Comput.* **2007**, *3*, 1803–1817.

[3] Cerezo, J.; Prampolini, G.; Cacelli, I. Developing accurate intramolecular force fields for conjugated systems through explicit coupling terms *Theor. Chem. Acc.* **2018**, *137*, 80.

[4] De Mitri, N.; Monti, S.; Prampolini, G.; Barone, V. Absorption and Emission Spectra of a Flexible Dye in Solution: A Computational Time-Dependent Approach *J. Chem. Theory Comput.* **2013**, *9*, 4507–4516.

[5] Cerezo, J.; Aranda, D.; Avila Ferrer, F. J.; Prampolini, G.; Santoro, F. Adiabatic-Molecular Dynamics Generalized Vertical Hessian Approach: A Mixed Quantum Classical Method to Compute Electronic Spectra of Flexible Molecules in the Condensed Phase *J. Chem. Theory Comput.* **2020**, *16*, 1215–1231.

[6] Cerezo, J.; Garcia Iriepa, C.; Santoro, F.; Navizet, I.; Prampolini, G. Unraveling the contributions to the spectral shape of flexible dyes in solution: insights on the absorption spectrum of an oxyluciferin analogue. *Phys. Chem. Chem. Phys.* **2023**, *25*, 5007–5020.

[7] Cerezo, J.; Gao, S.; Armaroli, N.; Ingrosso, F.; Prampolini, G.; Santoro, F.; Ventura, B.; Pastore, M. Non-Phenomenological Description of the Time-Resolved Emission in Solution with Quantum-Classical Vibronic Approaches. Application to Coumarin C153 in Methanol *Molecules* **2023**, *28*, 3910.

[8] Prampolini, G.; Ingrosso, F.; Segalina, A.; Caramori, S.; Foggi, P.; Pastore, M. Dynamical and Environmental Effects on the Optical Properties of an Heteroleptic Ru(II)–Polypyridine Complex: A Multilevel Approach Combining Accurate Ground and

Excited State QM-Derived Force Fields, MD and TD-DFT *J. Chem. Theory Comput.* **2019**, *15*, 529–545.

[9] Prampolini, G.; Ingrosso, F.; Cerezo, J.; Iagatti, A.; Foggi, P.; Pastore, M. Short- and Long-Range Solvation Effects on the Transient UV–Vis Absorption Spectra of a Ru(II)–Polypyridine Complex Disentangled by Nonequilibrium Molecular Dynamics *J. Phys. Chem. Lett.* **2019**, *10*, 2885–2891.

[10] Prampolini, G.; Andersen, A.; Poulter, B. I.; Khalil, M.; Govind, N.; Biasin, E.; Pastore, M. Integrated Quantum-Classical Protocol for the Realistic Description of Solvated Multinuclear Mixed-Valence Transition-Metal Complexes and Their Solvatochromic Properties *J. Chem. Theory Comput.* **2024**, *20*, 1306–1323.

[11] Barone, V.; Cacelli, I.; De Mitri, N.; Licari, D.; Monti, S.; Prampolini, G. Joyce and Ulysses: integrated and user-friendly tools for the parameterization of intramolecular force fields from quantum mechanical data *Phys. Chem. Chem. Phys.* **2013**, *15*, 3736–3751.

[12] Tomasi, J.; Mennucci, B.; Cammi, R. Quantum Mechanical Continuum Solvation Models *Chem. Rev.* **2005**, *105*, 2999–3094.

[13] Yaghoubi Jouybari, M.; Liu, Y.; Improta, R.; Santoro, F. Ultrafast Dynamics of the Two Lowest Bright Excited States of Cytosine and 1-Methylcytosine: A Quantum Dynamical Study *J. Chem. Theory Comput.* **2020**, *16*, 5792–5808; Publisher: American Chemical Society.

[14] Green, J. A.; Yaghoubi Jouybari, M.; Asha, H.; Santoro, F.; Improta, R. Fragment Diabatization Linear Vibronic Coupling Model for Quantum Dynamics of Multichromophoric Systems: Population of the Charge-Transfer State in the Photoexcited Guanine–Cytosine Pair *Journal of Chemical Theory and Computation* **2021**, *17*, 4660–4674; PMID: 34270258.

[15] Segalina, A.; Aranda, D.; Green, J. A.; Cristino, V.; Caramori, S.; Prampolini, G.; Pastore, M.; Santoro, F. How the Interplay among Conformational Disorder, Solvation, Local, and

Charge-Transfer Excitations Affects the Absorption Spectrum and Photoinduced Dynamics of Perylene Diimide Dimers: A Molecular Dynamics/Quantum Vibronic Approach *J. Chem. Theory Comput.* **2022**, *18*, 3718–3736; PMID: 35377648.

[16] Worth, G. Quantics: A general purpose package for quantum molecular dynamics simulations *Comput. Phys. Commun.* **2020**, *248*, 107040.

[17] García-Iriepa, C.; Gosset, P.; Berraud-Pache, R.; Zemmouche, M.; Taupier, G.; Dorkenoo, K. D.; Didier, P.; Léonard, J.; Ferré, N.; Navizet, I. Simulation and Analysis of the Spectroscopic Properties of Oxyluciferin and Its Analogues in Water *J. Chem. Theory Comput.* **2018**, *14*, 2117–2126.

[18] Isborn, C. M.; Mar, B. D.; Curchod, B. F. E.; Tavernelli, I.; Martínez, T. J. The Charge Transfer Problem in Density Functional Theory Calculations of Aqueously Solvated Molecules *J. Phys. Chem. B* **2013**, *117*, 12189–12201; PMID: 23964865.

[19] Cerezo, J.; Gierschner, J.; Santoro, F.; Prampolini, G. Explicit Modelling of Spectral Bandshapes by a Mixed Quantum-Classical Approach: Solvent Order and Temperature Effects in the Optical Spectra of Distyrylbenzene *ChemPhysChem* **2024**, *25*, e202400307.